

Cavity optomechanics in gallium phosphide microdisks

Matthew Mitchell,^{1,2} Aaron C. Hryciw,² and Paul E. Barclay^{1,2,*}

¹*Institute for Quantum Science and Technology, University of Calgary, Calgary, AB, T2N 1N4, Canada*

²*National Institute for Nanotechnology, 11421 Saskatchewan Dr. NW, Edmonton, AB T6G 2M9, Canada*

We demonstrate gallium phosphide (GaP) microdisk optical cavities with intrinsic quality factors $> 2.8 \times 10^5$ and mode volumes $< 10(\lambda/n)^3$, and study their nonlinear and optomechanical properties. For optical intensities up to 8.0×10^4 intracavity photons, we observe optical loss in the microcavity to decrease with increasing intensity, indicating that saturable absorption sites are present in the GaP material, and that two-photon absorption is not significant. We observe optomechanical coupling between optical modes of the microdisk around $1.5 \mu\text{m}$ and several mechanical resonances, and measure an optical spring effect consistent with a theoretically predicted optomechanical coupling rate $g_0/2\pi \sim 30 \text{ kHz}$ for the fundamental mechanical radial breathing mode at 488 MHz .

Cavity optomechanics provides a platform for exquisitely controlling coherent interactions between photons and mesoscopic mechanical excitations [1, 2]. Nanophotonic implementations of cavity optomechanics have recently been used to demonstrate laser cooling[3–6], optomechanically induced transparency[7, 8], and coherent wavelength conversion [9–11]. These experiments were enabled by photonic micro- and nanocavities engineered to minimize optical and mechanical dissipation rates, γ_o and γ_m respectively, while enhancing the single-photon optomechanical coupling rate, g_0 . The degree of coherent coupling between photons and phonons in these devices is often described by the cooperativity parameter, $C = Ng_0^2/\gamma_o\gamma_m$, which may exceed unity in several cavity optomechanics systems under investigation[2] for a sufficiently large intracavity photon number, N . Of particular promise are nanophotonic cavity optomechanical systems realized from semiconductors, such as silicon optomechanical crystals [5, 12] and gallium arsenide microdisks [13], owing to the tight optical confinement and large g_0 possible in these high refractive index contrast structures. Increasing C (above, for example, the value of $C \sim 20$ demonstrated in optomechanical crystals [14]), would enable improved bandwidth of coherent wavelength conversion [9], observation of normal mode splitting [15], and faster optomechanical cooling [5]. However, in these semiconductor-based large- g_0 devices, N is clamped by two-photon absorption[16, 17]. Here we demonstrate a cavity optomechanical system realized in a high refractive index material which does not exhibit nonlinear optical loss at commonly used telecommunications wavelengths.

The optomechanical system studied in this letter, an example of which is shown in Fig. 1(a)–(c), is based on whispering-gallery mode microdisk optical cavities fabricated from gallium phosphide (GaP). GaP is a semiconductor with a desirable combination of high refractive index ($n_{\text{GaP}} \sim 3.05$ at 1550 nm) and large electronic bandgap (2.26 eV); it is therefore optically transparent from 550 nm to IR wavelengths and has low two-photon absorption at 1550 nm . Compared to other materials

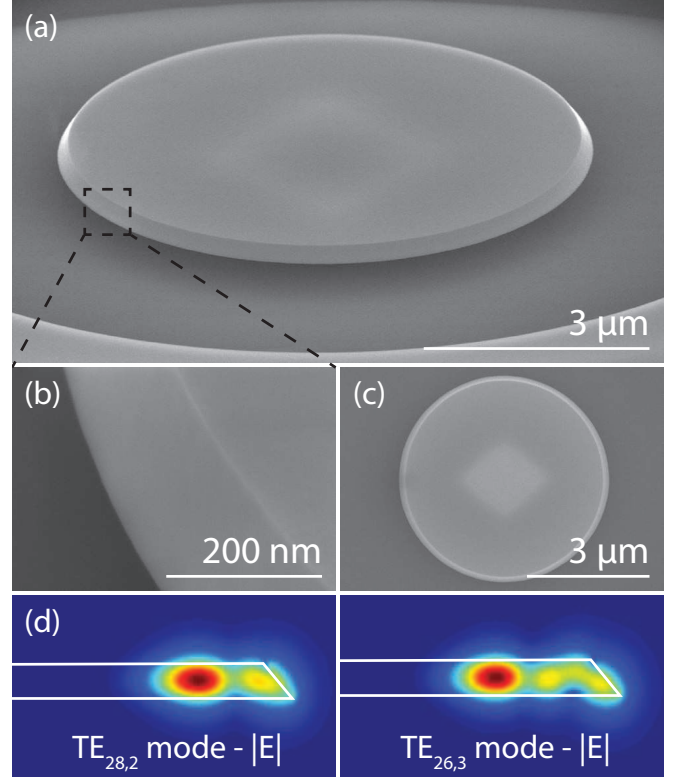


FIG. 1: (a)–(c) Scanning electron micrographs of a GaP microdisk resonator with a close-up of the disk sidewall. (d) Electric field distributions of the second ($n = 2$) and third ($n = 3$) radial order $\text{TE}_{m,n}$ microdisk modes, where m represents the azimuthal mode index and is chosen such that the mode wavelength is near 1550 nm .

with similar transparency windows used in cavity optomechanics, such as SiO_2 ($n_{\text{SiO}_2} = 1.45$) [3, 4, 7, 10], Si_3N_4 ($n_{\text{Si}_3\text{N}_4} = 2.0\text{--}2.2$) [11, 18] and AlN ($n_{\text{AlN}} = 2.0\text{--}2.2$) [19], GaP has a larger refractive index, enabling the fabrication of optical nanocavities with ultrasmall mode volumes[20, 21]. As such, GaP is a promising material for realizing cavity optomechanical systems with $g_0/2\pi$ approaching 1 MHz , as observed in Si and GaAs

devices [12–14, 22, 23]. In this letter, we show that GaP microcavities combine high optical quality factor $Q_i \sim 2.8 \times 10^5$, large optomechanical coupling $g_0/2\pi > 30$ kHz, and no observed two-photon absorption at 1550 nm band wavelengths. These properties allow the devices to operate close to the resolved-sideband regime with an intracavity photon number sufficient to allow observation of the optical spring effect.

The microdisks studied here were fabricated from an epitaxially grown wafer (supplied by IQE) consisting of a 250-nm-thick GaP device layer supported by a 750-nm-thick sacrificial aluminum gallium phosphide (AlGaP) layer and a GaP substrate. Microdisk patterns were defined using electron-beam lithography with ZEP520A resist, followed by a resist reflow step at 165 °C for 5 min. This step decreases imperfections in the circular electron-beam resist pattern, resulting in smoother sidewalls and an increased Q_i [24]. The resulting pattern was transferred into the GaP layer using a low-DC-bias inductively-coupled plasma reactive-ion etch with Ar/Cl₂ chemistry. The reflowed nature of the mask results in an angled GaP sidewall etch profile during this step, as seen in Figs. 1(a)–(c). This angle is not expected to limit Q_i in these devices, as microdisks with similar profiles [24, 25] have been reported with $Q_i > 10^6$ in other material systems. The resist was then removed with a 10 min deep-UV exposure (1.24 mW/cm² at 254 nm), followed by a 5 min soak in Remover PG®, and subsequent rinsing in acetone, isopropyl alcohol, and de-ionized water. The microdisks were undercut by selectively removing the AlGaP layer using a hydrofluoric acid wet etch (H₂O: 49% HF = 3:1). Microdisks with radii of $\sim 4 \mu\text{m}$ were studied in the work presented below.

The optomechanical properties of the microdisks were probed using a dimpled optical fiber taper [26] to evanescently couple light into and out of the cavity optical modes. The dimpled fiber taper was fabricated by modifying the process of Michael *et al.* [26] to use a ceramic edge as the dimple mold. The resulting dimple can be positioned within the optical near field of the microdisk, as shown in Fig. 2(b). Two tunable laser sources (New Focus Velocity) were used to measure the transmission of the fiber taper over the 1520–1625 nm wavelength range. The transmitted signal was split using a 10:90 fiber coupler, detected using low- (Newport 1621) and high-speed (Newport 1554-B) photodetectors, and recorded using a data acquisition card and a real-time spectrum analyser (Tektronix RSA5106A), respectively.

The optical response of a typical microdisk as a function of input wavelength, shown in Fig. 2(a) when the fiber taper dimple is positioned in the microdisk near field as in 2(b), consists of numerous resonances corresponding to excitation of high- Q_i whispering-gallery modes (WGMs) of the microdisk. The modal indices of each resonance, describing their azimuthal (m) and radial (n) order, were determined from comparisons of

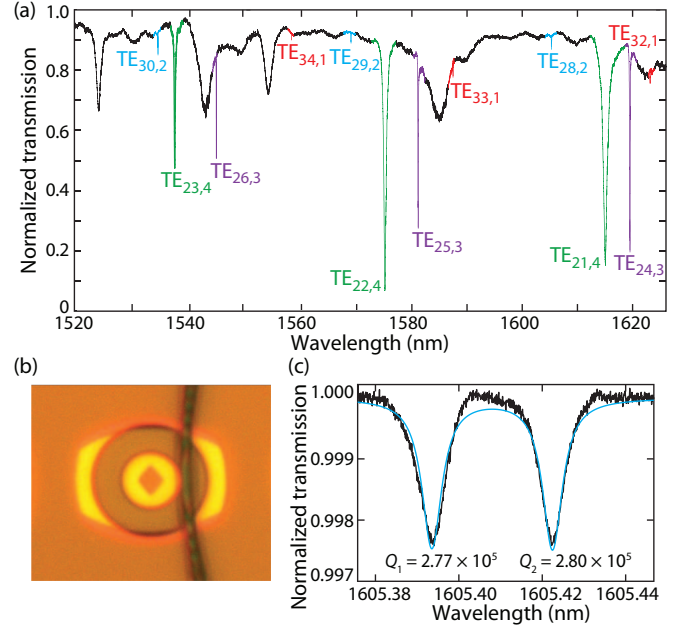


FIG. 2: (a) Fiber taper transmission spectrum of a GaP microdisk with a radius of $4 \mu\text{m}$, normalized by the fiber taper transmission when it is positioned far from the microdisk. Modes with common free spectral range are color coded and labeled as $\text{TE}_{m,n}$, with azimuthal and radial mode indices m and n , respectively. (b) Microscope image of dimpled fiber taper side-coupled to microdisk. (c) Narrow-wavelength scan of a high- Q_i mode, associated with the $[m, n] = 28, 2$ mode indices.

the measured Q_i and mode spacing with the mode spectrum predicted by finite-difference time-domain (FDTD) simulations [27] of the device. Note that this identification of azimuthal mode number should be considered approximate as our simulations used the nominal refractive index of GaP, and do not take into account perturbations to the refractive index from material impurities. For the device geometry used here, only TE-like modes (electric field dominantly radially polarized) with fundamental vertical field profile have sufficiently high Q_i to be observed. Figure 2(c) displays the optical response of the highest- Q_i mode observed in the fabricated GaP microdisks, which has $Q_i \sim 2.8 \times 10^5$ with minimal fiber loading. These are the highest optical quality factors observed to date in GaP nanophotonic devices. A mechanism limiting $Q_i < 10^6$ in these disks is the pedestal height (750 nm), which is determined by the thickness of the AlGaP layer. The choice of AlGaP layer thickness was determined by material availability, and should be further optimized in future devices. The doublet resonance structure is a result of scattering and modal coupling from imperfections in the microdisk, and indicates that the observed modes are standing waves [28]. Based on the comparisons with simulations, this mode is predicted to have modal indices $[m, n] = [28, 2]$, field pro-

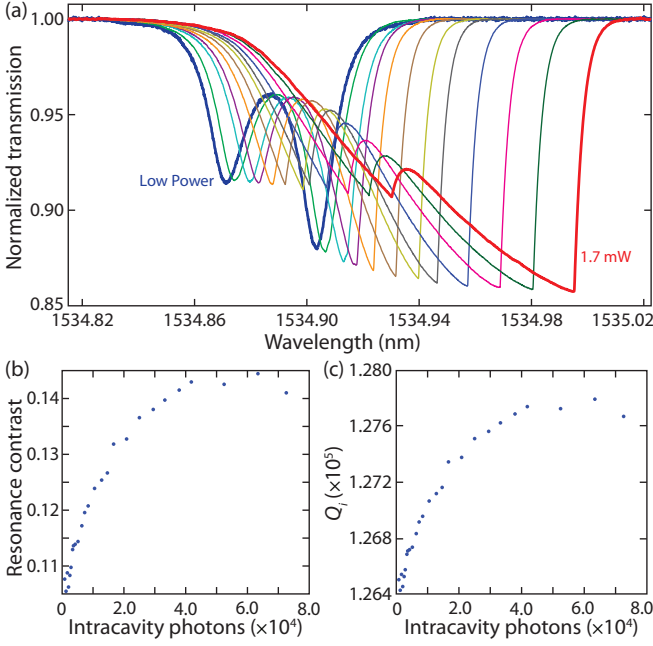


FIG. 3: (a) Optical response of the $\text{TE}_{30,2}$ mode, measured for varying input power P_i . (b) Measured resonance contrast ΔT_o , and (c) increase of intrinsic optical quality factor Q_i , as a function of intracavity photon number N , for the $\text{TE}_{34,1}$ mode.

file shown in Fig. 1(d), and standing-wave mode volume $V_o = 9.7(\frac{\lambda}{n_{\text{GaP}}})^3$.

To probe for nonlinear optical absorption in these microdisks, we measured their response as a function of fiber taper input power, P_i . Figure 3(a) shows the fiber taper transmission for varying P_i when the source laser is scanned with increasing wavelength across the $\text{TE}_{30,2}$ microdisk resonance. Although a power-dependent optical response is clearly observed, its behavior is indicative of a decrease in the internal optical loss of the microdisk, γ_i , with increasing P_i . This anomalous effect is illustrated in Fig. 3(b) for the $\text{TE}_{34,1}$ mode, which shows that the resonance contrast, $\Delta T_o = 4K/(1+K)^2$, increases with P_i , where $K = \gamma_e/(\gamma_e + \gamma_i(P_i))$, and γ_e is coupling rate between the microdisk standing wave mode and the forward- or backward-propagating fiber taper mode (i.e., $\gamma_o = \gamma_i + 2\gamma_e$). This is contrary to the behavior of cavities exhibiting multiphoton absorption, such as those fabricated from Si [16]. Figure 3(c) shows the corresponding increase of Q_i as a function of N , calculated according to:

$$\hbar\omega_{\text{cav}}N = \Delta T_o P_i \frac{Q_i}{\omega_{\text{cav}}}. \quad (1)$$

This effect may be the result of saturable absorbers in the microcavity, possibly in the form of O_2 -related impurities [29, 30] and will be investigated further in future work. A redshift in the cavity resonance wavelength λ_o ,

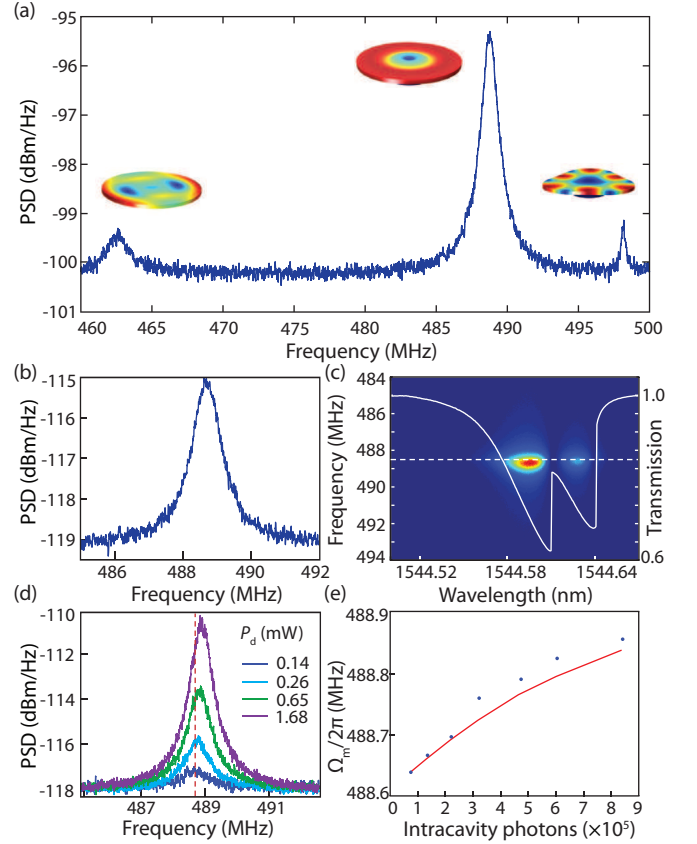


FIG. 4: Optomechanical data for a $4\text{ }\mu\text{m}$ radius GaP microdisk. (a) Electronic power spectral density (PSD) of photodetected taper transmission when ω_ℓ is blue detuned by $\sim \gamma_o/2$ from the $\text{TE}_{26,3}$ optical resonance. Simulated displacement amplitude profiles of the mechanical modes corresponding to the observed resonances in the PSD are also shown. (b) PSD of the fundamental RBM, measured for $P_i \sim 100\text{ }\mu\text{W}$. (c) Mechanical response of the RBM for varying laser wavelength for $P_i \sim 2.1\text{ mW}$. The corresponding transmission spectrum of the fiber taper evanescently coupled to the microdisk (white line), and low power RBM frequency (white dashed line), are also shown. (d) PSD of the fundamental RBM at four optical dropped powers when the laser was blue detuned by $\sim \gamma_o/2$ from ω_c . (e) Resonance frequency of the RBM as a function of intracavity photon number, when the laser was blue detuned by $\sim \gamma_o/2$ from ω_c . The solid red line represents predicted values from a theoretical model (see text).

is also observed with increasing P_i . This dispersive effect is the result of heating of the microcavity due to optical absorption, and can be suppressed by operating at lower temperatures [11].

To study the optomechanical properties of the microdisks, the effect of the thermal motion of the microdisk mechanical modes on the noise spectrum of the optical power transmitted through the fiber taper was measured. The dimensions of the microdisks were chosen to maximize g_0 and the mechanical frequency, Ω_m , of the fun-

damental radial breathing mode (RBM), without compromising Q_i . The $4\text{ }\mu\text{m}$ radius of the microdisks studied here is small enough to allow the mechanical breathing mode to have a high frequency ($\Omega_m/2\pi \sim 0.5\text{ GHz}$) and large enough to avoid optical radiation loss at a rate above other loss mechanisms of the microdisk. A typical spectrum, obtained in ambient conditions using the TE_{26,3} mode, with input laser frequency ω_ℓ blue detuned ($\omega_\ell \approx \omega_c + \gamma_o/2$), where ω_c is the cold cavity optical resonance frequency, is given in Fig. 4(a). Peaks associated with three mechanical resonances are visible; of particular interest is the fundamental RBM at $\Omega_m/2\pi = 488\text{ MHz}$. The RBM was found to have a mechanical zero-point fluctuation amplitude of 0.66 fm and displacement sensitivity of $4.43 \times 10^{-17}\text{ m}/\sqrt{\text{Hz}}$ for P_i of $\sim 600\text{ }\mu\text{W}$. The mode profiles of the mechanical resonances, and their effective mass[2], m_{eff} , were identified using COMSOL finite element simulations. The fundamental RBM ($m_{\text{eff}} = 40\text{ pg}$) was found to have a mechanical quality factor, measured at low P_i to avoid optical backaction effects, of $Q_m \sim 640$, while the $\Omega_m/2\pi = 462\text{ MHz}$ and $\Omega_m/2\pi = 498\text{ MHz}$ modes have $Q_m \sim 360$ and 450 , respectively. Q_m can be improved by engineering the device geometry and testing environment. While the RBM should not be limited by squeeze film damping, operation in vacuum could increase Q_m by eliminating air damping [31–34]. Mechanical clamping and phonon radiation loss can be reduced by further undercutting the microdisks to create ultra-small pedestals [11, 35, 36]. Phononic Bragg mirror inspired pedestal structures as seen in Ref.[36] could also be used to reduce clamping losses. This would require the growth of hetero-structured wafers, which would also allow control over pedestal height, as well as provide an opportunity to reduce impurities present in the current device layer. Through a combination of these techniques a 10^2 increase in Q_m is reasonable.

The optomechanical coupling coefficient G and rate g_0 [2, 12] between the fundamental RBM and the various optical WGMs of the microdisk were calculated using COMSOL finite element simulations and are given in Table I. For the devices under study, $g_0/2\pi \sim 30\text{ kHz}$ and $G/2\pi \sim 50\text{ GHz/nm}$ are comparable to record values[13]. The realizable cooperativity parameter for this device can be predicted from g_0 and the measured dissipation rates, $\gamma_m/2\pi \sim 7.63 \times 10^5\text{ Hz}$ and $\gamma_o/2\pi \sim 6.68 \times 10^8\text{ Hz}$, of the high- Q_i TE_{28,2} mode. These rates correspond to a single-photon cooperativity of $\sim 1.3 \times 10^{-6}$, which is on the same order of magnitude as similar WGM microcavity devices [2–4]. It is predicted that $C > 1$ for $N > 7.53 \times 10^5$ intracavity photons for the TE_{28,2} mode. The largest experimental C inferred was $C \sim 0.53$ for the TE_{30,2} mode, with $N \sim 4.15 \times 10^5$ (corresponding to $\sim 700\text{ }\mu\text{W}$ of dropped power). Note that this C is not a fundamental limit of our system, as C can be enhanced in future by improving the fiber–microdisk coupling efficiency or increasing P_i .

TABLE I: Simulated (FDTD) radiation-loss-limited optical quality factor for substrate-free and substrate-limited cases ($Q_{\text{rad}}^{\text{free}}$ and $Q_{\text{rad}}^{\text{sub}}$, respectively), measured intrinsic optical quality factors (Q_i), and simulated optomechanical coupling parameters for fundamental RBM ($\Omega_m/2\pi = 488\text{ MHz}$), for select measured optical modes.

Mode	$Q_{\text{rad}}^{\text{free}}$	$Q_{\text{rad}}^{\text{sub}}$	Q_i	$G/2\pi\text{ (}\frac{\text{GHz}}{\text{nm}}\text{)}$	$g_0/2\pi\text{ (kHz)}$
TE _{33,1}	$> 10^8$	1.1×10^6	2.6×10^5	48	31
TE _{28,2}	$> 10^8$	3.9×10^5	2.8×10^5	40	26
TE _{25,3}	6.0×10^7	1.4×10^5	0.9×10^5	35	23
TE _{22,4}	1.8×10^5	2.1×10^4	0.5×10^4	32	21

The measurement noise background in Fig. 4 was dominated by detector noise ($\sqrt{S_{xx}^{DET}} \sim 2 \times 10^{-17}\text{ m}/\sqrt{\text{Hz}}$), and shot noise ($\sqrt{S_{xx}^{SN}} \sim 5 \times 10^{-18}\text{ m}/\sqrt{\text{Hz}}$). This noise level is roughly a factor of 100 times the standard quantum limited displacement noise ($\sqrt{S_{xx}^{SQL}} = 6 \times 10^{-19}\text{ m}/\sqrt{\text{Hz}}$). For the current device, at higher operating P_i , where optomechanical backaction noise is equal to shot noise ($S_{xx}^{BA} = S_{xx}^{SN}$), detector noise will remain dominant. As such, detection of the RBM with SQL precision using the TE_{26,3} optical mode, would require lower noise photodetection. Alternatively, using higher Q_i modes such as the TE_{28,2} mode in Fig. 2(c), would further increase the measurement precision. However, reaching the SQL using these high- Q_i modes will not be possible without significantly improved fiber coupling efficiency, as critical coupling is a requirement for SQL measurements [2].

We further explored the optomechanical coupling by measuring the dependence of the lineshape of the fundamental RBM on N . Figure 4(c) illustrates the dependence of the mechanical spectrum on laser wavelength as it is swept across the TE_{26,3} optical cavity resonance, at a fixed $P_i = 2.1\text{ mW}$. As the laser approaches the cavity resonance and N increases, Ω_m is observed to increase by up to 250 kHz . This is the result of the optical spring effect, and is further illustrated in Figs. 4(d) and (e), which show the effect of varying P_i for fixed $\omega_\ell = \omega_c + \gamma_o/2$. Note that for $P_i \gg 200\text{ }\mu\text{W}$, ω_c red-shifts due to the heating of the microdisk by the intracavity saturable absorption described above. The fit in Fig. 4(e) was obtained using the model for the optical spring effect described by Aspelmeyer *et al.* [2], taking into account the measured dependence of $\Delta\omega = \omega_\ell - \omega_c$, and ΔT_o on N . The observed power dependent shift in Ω_m of up to 218 kHz is in good agreement with this model. We also observe mechanical damping while blue detuned from the cavity resonance, as can be observed from Fig. 4(d). This effect is a result of thermo-optic damping[18, 37]. For small N , the TE_{26,3} mode used in these spring effect measurements had an intrinsic $Q_i \sim 6.3 \times 10^4$ and a resonance contrast of $\Delta T_o \sim 0.63$. From FDTD simulations, this mode is predicted to have a standing-wave mode volume of $V_o = 11.1(\frac{\lambda}{n_{\text{GaP}}})^3$ and the field profile shown in Fig.

1(d).

For optomechanical cooling of a mechanical resonator, it is desirable to be in the sideband-resolved regime [3, 35]. In our case, the optical linewidth of the highest- Q_i mode is $\gamma_o/2\pi \sim 668$ MHz. As seen in Table I, our measured Q_i values are significantly lower than the radiation-loss-limited quality factor, $Q_{\text{rad}}^{\text{sub}}$, which includes leakage into the substrate. We also observe that the $\text{TE}_{33,1}$ and $\text{TE}_{28,2}$ modes have similar Q_i , despite the lower predicted radiation loss of the $\text{TE}_{33,1}$ mode. This suggests that either material absorption or surface scattering is placing the upper limit on Q_i for these devices. The sideband-resolved regime may be attainable through further optimization of Q_i by fabricating devices from wafers with a thicker sacrificial AlGaP layer and lower GaP linear absorption, and with reduced surface roughness.

In conclusion, we have fabricated GaP microdisks with the highest intrinsic optical quality factors to date ($Q_i > 2.8 \times 10^5$) and have demonstrated the first instance of cavity optomechanics in GaP devices. The observed increase in Q_i with input power, paired with the absence of nonlinear absorption for $N > 10^5$, illustrates the potential that GaP holds for experiments in quantum optomechanics. These devices are also promising for implementing high-frequency cavity optomechanics at visible wavelengths and for applications in nonlinear optics.

We would like to thank Marcelo Wu, David Lake, Behzad Khanaliloo, and Chris Healey for helpful discussions. We would also like to express gratitude to Charles Santori, Kai-Mei C. Fu, and Hewlett-Packard Labs for valuable contributions providing and characterizing the GaP material. This work was supported by NRC, CFI, iCORE/AITF, and NSERC.

* Electronic address: pbarclay@ucalgary.ca

- [1] T. Kippenberg and K. Vahala, “Cavity Opto-mechanics,” *Opt. Express* **15**, 17 172–17 205 (2007).
- [2] M. Aspelmeyer, T. J. Kippenberg, and F. Marquardt, “Cavity Optomechanics,” *arXiv preprint arXiv:1303.0733* (2013).
- [3] Y.-S. Park and H. Wang, “Resolved-sideband and cryogenic cooling of an optomechanical resonator,” *Nature Phys.* **5**, 489–493 (2009).
- [4] A. Schliesser, O. Arcizet, R. Rivière, G. Anetsberger, and T. Kippenberg, “Resolved-sideband cooling and position measurement of a micromechanical oscillator close to the Heisenberg uncertainty limit,” *Nature Phys.* **5**, 509–514 (2009).
- [5] J. Chan, T. P. M. Alegre, A. H. Safavi-Naeini, J. T. Hill, A. Krause, S. Groblacher, M. Aspelmeyer, and O. Painter, “Laser cooling of a nanomechanical oscillator into its quantum ground state,” *Nature* **478**, 89–92 (2011).
- [6] A. Safavi-Naeini, J. Chan, J. Hill, T. P. M. Alegre, A. Krause, and O. Painter, “Observation of quantum motion of a nanomechanical resonator,” *Phys. Rev. Lett.* **108**, 033 602 (2012).
- [7] S. Weis, R. Rivière, S. Deléglise, E. Gavartin, O. Arcizet, A. Schliesser, and T. J. Kippenberg, “Optomechanically induced transparency,” *Science* **330**, 1520–1523 (2010).
- [8] A. H. Safavi-Naeini, T. M. Alegre, J. Chan, M. Eichenfield, M. Winger, Q. Lin, J. T. Hill, D. Chang, and O. Painter, “Electromagnetically induced transparency and slow light with optomechanics,” *Nature* **472**, 69–73 (2011).
- [9] J. T. Hill, A. H. Safavi-Naeini, J. Chan, and O. Painter, “Coherent optical wavelength conversion via cavity optomechanics,” *Nat. Commun.* **3**, 1196 (2012).
- [10] C. Dong, V. Fiore, M. C. Kuzyk, and H. Wang, “Optomechanical dark mode,” *Science* **338**, 1609–1613 (2012).
- [11] Y. Liu, M. Davanço, V. Aksyuk, and K. Srinivasan, “Electromagnetically Induced Transparency and Wideband Wavelength Conversion in Silicon Nitride Microdisk Optomechanical Resonators,” *Phys. Rev. Lett.* **110**, 223 603 (2013).
- [12] M. Eichenfield, J. Chan, R. Camacho, K. Vahala, and O. Painter, “Optomechanical crystals,” *Nature* **462**, 78–82 (2009).
- [13] L. Ding, C. Baker, P. Senellart, A. Lemaitre, S. Ducci, G. Leo, and I. Favero, “High frequency GaAs nanomechanical disk resonator,” *Phys. Rev. Lett.* **105**, 263 903 (2010).
- [14] J. Chan, A. Safavi-Naeini, J. Hill, S. Meenehan, and O. Painter, “Optimized Optomechanical Crystal Cavity with Acoustic Radiation Shield,” *Appl. Phys. Lett.* **101**, 081 115 (2012).
- [15] S. Gröblacher, K. Hammerer, M. R. Vanner, and M. Aspelmeyer, “Observation of strong coupling between a micromechanical resonator and an optical cavity field,” *Nature* **460**, 724–727 (2009).
- [16] P. E. Barclay, K. Srinivasan, and O. Painter, “Nonlinear response of silicon photonic crystal microresonators excited via an integrated waveguide and a fiber taper,” *Opt. Express* **13**, 801–820 (2005).
- [17] X. Sun, X. Zhang, C. Schuck, and H. X. Tang, “Nonlinear optical effects of ultrahigh-Q silicon photonic nanocavities immersed in superfluid helium,” *Sci. Rep.* **3** (2013).
- [18] M. Eichenfield, R. Camacho, J. Chan, K. J. Vahala, and O. Painter, “A picogram- and nanometre-scale photonic-crystal optomechanical cavity,” *Nature* **459**, 550–555 (2009).
- [19] C. Xiong, X. Sun, K. Y. Fong, and H. X. Tang, “Integrated high frequency aluminum nitride optomechanical resonators,” *Appl. Phys. Lett.* **100**, 171 111–171 111 (2012).
- [20] K. Rivoire, A. Faraon, and J. Vučković, “Gallium phosphide photonic crystal nanocavities in the visible,” *Appl. Phys. Lett.* **93**, 063 103 (2008).
- [21] P. E. Barclay, K. M. C. Fu, C. Santori, A. Faraon, and R. G. Beausoleil, “Hybrid nanocavities for resonant enhancement of color center emission in diamond,” *Phys. Rev. X* **1**, 011 007 (2011).
- [22] L. Ding, C. Baker, P. Senellart, A. Lemaitre, S. Ducci, G. Leo, and I. Favero, “Wavelength-sized GaAs optomechanical resonators with gigahertz frequency,” *Appl. Phys. Lett.* **98** (2011).
- [23] X. Sun, J. Zhang, M. Poot, C. Wong, and H. Tang, “Femtogram Doubly Clamped Nanomechanical Resonators Embedded in a High-Q Two-dimensional Photonic Crys-

- tal Nanocavity,” *Nano Lett.* **12**, 2299–2305 (2012).
- [24] M. Borselli, T. J. Johnson, and O. Painter, “Beyond the Rayleigh scattering limit in high-Q silicon microdisks: theory and experiment,” *Opt. Express* **13**, 1515–1530 (2005).
- [25] P. E. Barclay, B. Lev, K. Srinivasan, H. Mabuchi, and O. Painter, “Integration of fiber coupled high-Q SiNx microdisks with atom chips,” *Appl. Phys. Lett.* **89**, 131 108 (2006).
- [26] C. P. Michael, M. Borselli, T. J. Johnson, C. Chrystala, and O. Painter, “An optical fiber-taper probe for wafer-scale microphotonic device characterization,” *Opt. Express* **15**, 4745–4752 (2007).
- [27] A. F. Oskooi, D. Roundy, M. Ibanescu, P. Bermel, J. Joannopoulos, and S. G. Johnson, “Meep: A flexible free-software package for electromagnetic simulations by the FDTD method,” *Comp. Phys. Comm.* **181**, 687–702 (2010).
- [28] M. Borselli, K. Srinivasan, P. E. Barclay, and O. Painter, “Rayleigh scattering, mode coupling, and optical loss in silicon microdisks,” *Appl. Phys. Lett.* **85**, 3693–3695 (2004).
- [29] P. J. Dean and C. H. Henry, “Electron-Capture (”Internal”) Luminescence from the Oxygen Donor in Gallium Phosphide,” *Phys. Rev.* **176**, 928–937 (1968).
- [30] P. Dean, C. Henry, and C. Frosch, “Infrared Donor-Acceptor Pair Spectra Involving the Deep Oxygen Donor in Gallium Phosphide,” *Phys. Rev.* **168**, 812 (1968).
- [31] R. Rivière, *Cavity optomechanics with silica toroidal microresonators down to low phonon occupancy*, Ph.D. thesis, Ludwig-Maximilians-Universität München (2011).
- [32] X. Sun, X. Zhang, and H. X. Tang, “High-Q silicon optomechanical microdisk resonators at gigahertz frequencies,” *Appl. Phys. Lett.* **100**, – (2012).
- [33] O. Svitelskiy, V. Sauer, D. Vick, K.-M. Cheng, N. Liu, M. R. Freeman, and W. K. Hiebert, “Nanoelectromechanical devices in a fluidic environment,” *Phys. Rev. E* **85**, 056 313 (2012).
- [34] D. Parrain, C. Baker, T. Verdier, P. Senellart, A. Lemaitre, S. Ducci, G. Leo, and I. Favero, “Damping of optomechanical disks resonators vibrating in air,” *Appl. Phys. Lett.* **100** (2012).
- [35] A. Schliesser, R. Riviere, G. Anetsberger, O. Arcizet, and T. J. Kippenberg, “Resolved-sideband cooling of a micromechanical oscillator,” *Nature Phys.* **4**, 415–419 (2008).
- [36] D. T. Nguyen, C. Baker, W. Hease, S. Sevil, P. Senellart, A. Lematre, S. Ducci, G. Leo, and I. Favero, “Ultrahigh Q-frequency product for optomechanical disk resonators with a mechanical shield,” *Appl. Phys. Lett.* **103** (2013).
- [37] K. Srinivasan, H. Miao, M. Rakher, M. Davanço, and V. Aksyuk, “Optomechanical transduction of an integrated silicon cantilever probe using a microdisk resonator,” *Nano Lett.* **11**, 791 (2011).